metals

MDPI

Article

Equation of State for Aluminum at High Entropies and Internal Energies in Shock Waves

Konstantin V. Khishchenko *, Kseniya A. Boyarskikh, Liliya R. Obruchkova and Nikolai N. Seredkin

Joint Institute for High Temperatures of the Russian Academy of Sciences, Izhorskaya 13 Bldg 2, Moscow 125412, Russia
* Correspondence: konst@ihed.ras.ru

Abstract

The present theoretical work is devoted to the construction of a model of the equation of state for matter, where the specific volume is used as the thermodynamic potential, and the entropy and the thermal part of the internal energy act as thermodynamic variables. Based on the proposed model, called STEC, calculations were carried out for aluminum in the region of high internal energies and entropies. A comparison of the calculated shock adiabats with the available data from shock-wave experiments indicates that the constructed equation of state describes well the thermodynamic properties of aluminum up to a shock compression pressure of about 1 TPa. The proposed STEC equation-of-state model can be used in numerical simulations of various processes under extreme conditions at high energy densities.

Keywords: equation of state; aluminum; shock wave; high entropies; high internal energies; high energy densities

check for updates

Received: 11 September 2025
Revised: 13 October 2025
Accepted: 21 October 2025
Published: 25 October 2025

Citation: Khishchenko, K.V.; Boyarskikh, K.A.; Obruchkova, L.R.; Seredkin, N.N. Equation of State for Aluminum at High Entropies and Internal Energies in Shock Waves. *Metals* **2025**, *15*, 1189. https://doi.org/10.3390/met15111189

Copyright: © 2025 by the authors. Licensee MDPI, Basel, Switzerland. This article is an open access article distributed under the terms and conditions of the Creative Commons Attribution (CC BY) license (https://creativecommons.org/licenses/by/4.0/).

1. Introduction

The theoretical description of the behavior of matter across a wide range of changes in thermodynamic variables is of interest for solving a broad range of problems in fundamental and applied physics of intense pulsed processes [1–3]. The impact of high mechanical and thermal loads upon a material leads to a change in the parameters of its state from the starting point towards an increase in internal energy. And this can be accompanied by a noticeable increase in pressure, for example, as occurs during a high-velocity collision of bodies [4–15] or during high-intensity short laser irradiation of a solid target [16–30], or a noticeable increase in temperature and entropy, for example, as during an electrical explosion of conductors under the influence of a powerful current pulse [31–37]. For numerical modeling of such fast-moving processes, it is necessary to know the equation of state for the substance under consideration in the entire range of realized parameters [38–40]. Moreover, the correctness of the equation of state will play a decisive role in ensuring that the modeling results are correct [5,6,20,25,32,41,42].

Aluminum is an example of a material that is widely used as an element of structures that are subject to intense impulse effects during operation [4,12,13,15,43]. In particular, aluminum was the main material for the protective shields (screens) of the Vega unmanned spacecraft against impacts from dust particles moving at a velocity of 60 to 80 km/s during the exploration of Halley's Comet [4]. In developing the optimal design of these screens, the equation of state for aluminum was used, taking into account melting and evaporation [2,4,44], which was important for the correct numerical modeling of the impact of dust

particles with the screen at such velocities. For calculating the parameters of aluminum screens for protecting spacecraft from space debris at lower impact velocities (from 3 to 15 km/s), a simpler equation of state (without taking into account phase transformations) was used in a recent study [13]. A review of some of the works related to protecting spacecraft from space debris can be found elsewhere [12].

A numerical simulation of the impact of an aluminum cylinder with a velocity of 6.6 km/s on an aluminum plate was carried out [5] using the equation of state in three different versions, namely, in caloric form for condensed and rarefied matter [45] and in a form based on the thermodynamic potential of the Helmholtz free energy [2] taking into account melting and evaporation, not allowing or allowing the possibility of the formation of metastable states of liquid and vapor phases. Moreover, the results of modeling [5] with the first and third variants of the equation of state turned out to be similar. To simulate the impact of a titanium plate with a velocity of about 10.4 km/s on a static aluminum plate, in addition to the equation of state [2], which takes into account phase transformations and metastable regions, models of the kinetics of the formation of a liquid–vapor mixture and the mechanical fracture of a metastable liquid were taken into account [6].

For simulating the impact of an aluminum ball with velocities ranging from 2 to 6.5 km/s with targets in the form of round plates made of high-density polyethylene, the equation of state for both materials was used in a simple caloric form together with the constitutive relations and the fracture model [46]. A discrepancy was noted between the simulation results and the experimental data at impact velocities above 5.5 km/s, possibly due to the simplified form of the equation of state used without taking into account the effects of liquid phase formation [46].

Models of the dynamics of shock-wave loading processes in aluminum samples were implemented taking into account plasticity and fragmentation through the dynamics and kinetics of microdefects (dislocations and microcracks) [11], as well as in viscoelastic and hydrodynamic approximations [9]. In the first case [11], the model also included the equation of state for aluminum taking into account melting [2], and in the second case [9], a simpler model of the equation of state for the condensed phase of this metal (without taking into account melting) [47] was used.

Numerical studies of shock loading processes in initially porous aluminum samples of conical shape, inserted into a solid target (with a conical cavity) made of metal with higher dynamic impedance (steel and lead), made it possible to establish some features of the resulting flow with a converging shock wave [7,8]. In these studies, the equation of state for aluminum (as well as for other metals) was used within the framework of the model [2] that takes into account melting (at the compression stage) and evaporation (at the jet expansion stage, in the target version with an outlet hole [8]).

In the practice of shock-wave experiments, aluminum is frequently used as a standard material with well-studied properties [48]. However, a noticeable discrepancy between the experimental points for the shock compressibility of aluminum occurs at pressures above 0.2 TPa [49,50], possibly due to a discrepancy in the parameters of the shock adiabats of other standard materials available in this region. Calculations using the Thomas–Fermi (with corrections) and Hartree–Fock–Slater models were carried out to refine the equation of state [50,51], and an interpretation of the available data from shock-wave experiments for this metal in the region of higher pressures has been given [51].

Aluminum is widely used as a component of composites (for example, ceramic filler in an aluminum matrix [52], carbon fiber-reinforced plastics between aluminum plates bonded by epoxy adhesive [53] and compositions of layers of elastomeric polyurethane and honeycomb aluminum [54]) and other materials (for example, foams [55–58]) for structures subject to high dynamic loads.

A numerical model of the ablation process of an aluminum target under the action of an ultrashort (femtosecond) high-intensity laser pulse was proposed [18] taking into account the absorption of radiation energy, the effects of electron thermal conductivity and the exchange of electron energy with phonons or ions, phase transformations (melting and evaporation), and the possibility of forming metastable states of the target material under tensile stresses. The equation of state in such problems [18,20] was used in a variant with a distinction between the temperatures of the electronic and ionic subsystems, and for the ionic subsystem a model approach based on some ideas [1,2] was implemented.

Irradiation of plates made of aluminum and AMg6M alloy with short (picosecond) laser pulses allows, in experiments [19,23], the study of the phenomenon of spalling from the rear side of the target and also, using a hydrodynamic code, the calculation of the tensile mechanical stress at which this spalling occurred. In modeling this process [19,23], the equation of state for aluminum was used in caloric form [45]. The possibility of obtaining additional information about the equation of state for the material under study in such experiments has been considered elsewhere [22]. The use of other variants of the equations of state for aluminum in similar problems is also encountered [59].

The action of shock waves obtained by laser pulses has found application as a tool for surface treatment of metals (in particular, aluminum alloys [60–62]) by (laser shock) peening. Other methods of influencing the mechanical properties of metals are also being developed, such as stress relief using ultrasonic vibration [63]. To generalize experimental data in a form convenient for use in numerical modeling, in particular, different models of constitutive relations are used [63].

Aluminum and its alloys are technologically advanced materials for the production of conductive elements for various applications in high-current electronics. For example, a magnetic field created by a high-linear-density current pulse can be used to accelerate a duralumin plate [10], which can serve as an impactor in a shock-wave experiment. Aluminum foils are used in the form of cylindrical liners compressed by a magnetic field to produce hot, dense plasma [31,64]. A variant of the numerical model of the initial stage of this process was proposed in the work [31], in which the equation of state for aluminum was used, taking into account the phase transition of the solid phase into liquid and then the formation of a two-phase liquid–vapor mixture and plasma [2,4,44]. The possible development of instabilities (capable of preventing the achievement of the desired parameters of dense hot plasma) during heating of thin aluminum foil in a vacuum by a high-density current pulse was investigated experimentally in a recent work [64]. Rapid heating of thin aluminum foil in transparent dielectric plates has been studied in experiments [32] and simulations (with different equations of state for aluminum) [32,41,42]; in this case, heating and expansion of the molten metal with the formation of plasma occur at a pressure higher than the critical point of the liquid–vapor phase transition.

Electrical explosions of aluminum wires in water were investigated in experiments [37], and the development of thermoelectric instabilities was discovered after the start of evaporation of the metal. Various methods of accelerating an aluminum disk using electrical explosion of thin foils (made of aluminum or copper) in water have been tested in experiments and simulations [40]. In hydrodynamic modeling [37,40], equations of state for the metals and water in caloric and thermal forms were used.

In addition to the equations of state [2,4,44,47,50,51,59] mentioned in the above cases for aluminum, there are many examples of using different model approaches to describe the thermodynamic properties of this metal at high energy densities [65–96]. These approaches are constantly being improved, and their adequacy is conveniently tested using the example of aluminum, for which there is a lot of experimental data over a wide range of pressures and internal energies obtained using shock-wave techniques. And these circumstances

stimulate an unquenchable interest in the study of this material, despite the feeling that it has already been thoroughly studied.

When solving problems of hydrodynamics, the equation of state closes the system of equations of motion of the medium, which express the laws of conservation of mass, momentum and energy. In this case, a necessary requirement for the equation of state is the expression of the relationship between density (ρ) or specific volume ($V = \rho^{-1}$), pressure (P) and specific internal energy (E). Examples of equations of state in the form

$$E = E(V, P) \tag{1}$$

or

$$P = P(V, E), \tag{2}$$

which agree well with data from shock-wave experiments, are known [9,33,45,92,97–100]. This caloric form of the equation of state is sufficient for modeling adiabatic processes [5,9,23,33,59,96].

Another convenient form of representing the equations of state [47,50,65–67,76,77,79,82,86,87,93,94,101,102] are the dependencies

$$E = E(V, T) \tag{3}$$

and

$$P = P(V, T), \tag{4}$$

which together also relate the specific volume, pressure and internal energy by means of an additional thermodynamic parameter—the absolute temperature (T) [103]. Knowledge of temperature expands the possibilities of constructing numerical models for processes with heat sources, for example, with the effect of thermal conductivity [104].

As is known [103], the relationship between the derivatives of functions (3) and (4) is established by the first and second laws of thermodynamics, which express the law of conservation of energy in a thermodynamic system during a reversible process:

$$\mathrm{d}E = -P\mathrm{d}V + T\mathrm{d}S, \tag{5}$$

where S is the specific entropy. This relationship can be transformed to a form with the variables V and T, which connects the derivatives of the functions (3) and (4) [103]. This can become the basis for finding the temperature from the equation of state (1) or (2) if one involves some additional information about the temperature of the substance [1], for example, at the atmospheric pressure isobar [97] or an isochor [98]. Of course, the equation of state can be specified directly in the variables through whose differentials the total differential of the internal energy (5) is expressed, namely, in the canonical form $E = E(V, S)$ [105].

In this paper, based on the main thermodynamic law (5), a model of the equation of state for matter is proposed in which specific entropy and the thermal part of the specific internal energy are used as variables. A description of this model is given in Section 2. The results of calculating the thermodynamic characteristics of aluminum using the new model are given in comparison with the available data from shock-wave experiments at high pressures in Section 3. The main conclusions of this work are drawn in Section 4.

2. Equation-of-State Model

In a number of papers [77,86,87,106–109], the thermodynamic equilibrium component model, called TEC, has been proposed to describe properties of various materials at high pressures. The expressions of this model, given in the form of the caloric and thermal

equations of state (3) and (4), do not formally satisfy the main law (5) [109], but the results of calculations using this model demonstrate good agreement with shock-wave data, in particular, for aluminum [77,86,87]. In this section, the expressions of the TEC model are discussed, the issue of their inconsistency with the main law (5) is examined and a new model, called STEC (S stands for entropy), based on the main law (5) is proposed.

2.1. TEC Model

The pressure and specific internal energy in the TEC model are composed of two terms responsible for the cold (P_c and E_c) and thermal (P_t and E_t) parts:

$$P(V,T) = P_c(V) + P_t(V,T) \tag{6}$$

and

$$E(V,T) = E_c(V) + E_t(T). \tag{7}$$

The cold pressure is given in the form of the Murnaghan equation [110]:

$$P_c(V) = A(\sigma^n - 1), \tag{8}$$

where $\sigma = V_0/V$; V_0 is the specific volume of the substance at $P_c = 0$; and A and n are constants. The cold part of the internal energy is chosen from the conditions $P_c = -\mathrm{d}E_c/\mathrm{d}V$ and $E_c(V_0) = 0$:

$$E_c(V) = \frac{AV_0}{n-1}\left(\frac{\sigma^n - 1 + n}{\sigma} - n\right). \tag{9}$$

The thermal pressure is given in the following form:

$$P_t(V,T) = \frac{\Gamma}{V}C_{V0}(T - T_0), \tag{10}$$

where C_{V0} and T_0 are constants; Γ is a coefficient that depends only on temperature,

$$\Gamma(T) = \Gamma_\infty + \frac{\Gamma_0 - \Gamma_\infty}{1 + C_1(T - T_0)}, \tag{11}$$

Γ_0, Γ_∞ and C_1 are constants, and

$$C_1 = \frac{\Gamma_0 - \Gamma_1}{(T_1 - T_0)(\Gamma_1 - \Gamma_\infty)}, \tag{12}$$

where Γ_1 and T_1 are also constants. The thermal part of the specific internal energy is given as

$$E_t(T) = C_{V0}(T - T_0). \tag{13}$$

One can easily verify that the expressions (6)–(13) of the TEC model do not satisfy the main law (5). Directly from (5), the expression for the total differential of the entropy with respect to the variables E and V follows:

$$\mathrm{d}S = T^{-1}\mathrm{d}E + PT^{-1}\mathrm{d}V. \tag{14}$$

From (14), the relations $(\partial S/\partial E)_V = T^{-1}$ and $(\partial S/\partial V)_E = PT^{-1}$ follow in turn. By equating the mixed derivatives of entropy with respect to E and V, one can determine the relationship between the derivatives of functions (3) and (4):

$$(\partial E/\partial V)_T - T(\partial P/\partial T)_V + P = 0. \tag{15}$$

This relation for thermodynamically consistent equations of state (3) and (4) is an identity. For expressions (6)–(13) this requirement is not met.

Some illustrations of this thermodynamic inconsistency of the TEC model are given in Appendix A.

It should be noted that according to the definitions of the thermal parts of pressure (10) and internal energy (13), it turns out that the cold parts (8) and (9) correspond to the isotherm $T = T_0$.

2.2. STEC Model

Following the accepted thermodynamic definition of pressure, which succeeds from the main law (5),

$$P = -(\partial E/\partial V)_S, \tag{16}$$

the STEC model assumes that the cold parts of pressure (P_s) and specific internal energy (E_s) correspond to the isentrope $S = S_0$.

Then the pressure and internal energy are written as functions of specific volume and specific entropy:

$$P(V,S) = P_s(V) + P_t(V,S) \tag{17}$$

and

$$E(V,S) = E_s(V) + E_t(V,S). \tag{18}$$

The cold parts of pressure and specific internal energy are given similarly to (8) and (9):

$$P_s(V) = A(\sigma^n - 1) \tag{19}$$

and

$$E_s(V) = \frac{AV_0}{n-1}\left(\frac{\sigma^n - 1 + n}{\sigma} - n\right). \tag{20}$$

The thermal part of pressure is given similarly to (10) after eliminating temperature using (13):

$$P_t(V,S) = \frac{\Gamma_t}{V} E_t(V,S), \tag{21}$$

where

$$\Gamma_t(E_t) = \Gamma_\infty + \frac{\Gamma_0 - \Gamma_\infty}{1 + \mathrm{A}_1 E_t}, \tag{22}$$

Γ_0 and Γ_∞ are the same constants as in (11), and

$$\mathrm{A}_1 = \frac{C_1}{C_{V0}}, \tag{23}$$

where C_1 is the same constant as in (12).

To find the entropy dependence for the internal energy, it is assumed that the isochoric heat capacity at $V = V_0$ is a constant value, $C_V|_{V=V_0} = C_{V0}$. Then the thermal part of the internal energy at $V = V_0$ depends on the entropy as follows:

$$E_v(S) = C_{V0}T_0\left(\exp\frac{S - S_0}{C_{V0}} - 1\right). \tag{24}$$

By substituting the expressions (17) and (18) into the definition of pressure (16), one can obtain a differential equation for the relationship between E_t and V on an isentrope. By solving this equation taking into account (24), an explicit expression for the specific

volume as a function of the thermal part of the specific internal energy and the specific entropy can be obtained:

$$V(E_t, S) = V_0 \exp\left(\frac{1}{\Gamma_0} \ln \frac{E_v(S)}{E_t} + \frac{\Gamma_0 - \Gamma_\infty}{\Gamma_0 \Gamma_\infty} \ln \frac{\Gamma_0 + \Gamma_\infty \mathrm{A}_1 E_v(S)}{\Gamma_0 + \Gamma_\infty \mathrm{A}_1 E_t}\right). \tag{25}$$

This quantity V (25) can now be considered as a thermodynamic potential for which the total differential is expressed through the differentials of the variables E_t and S by transforming the basic law (5) taking into account relations (17) to (20):

$$\mathrm{d}V = -{P_t}^{-1}\mathrm{d}E_t + T{P_t}^{-1}\mathrm{d}S. \tag{26}$$

From this, the relations for the factors of the differentials of the variables on the right side of the expression for the differential $\mathrm{d}V$ (26) follow:

$${P_t}^{-1} = -(\partial V/\partial E_t)_S \tag{27}$$

and

$$T{P_t}^{-1} = (\partial V/\partial S)_{E_t}. \tag{28}$$

Applying relation (27) to the thermodynamic potential V (25) results in the expression (21). Applying relation (28) to the potential V (25) together with the formula for P_t (21) allows one to obtain an explicit expression for the temperature as a function of the variables E_t and S:

$$T(E_t, S) = T_0 \frac{\Gamma_t E_t}{\Gamma_v E_v(S)} \exp \frac{S - S_0}{C_{V0}}, \tag{29}$$

where

$$\Gamma_v(E_v) = \Gamma_\infty + \frac{\Gamma_0 - \Gamma_\infty}{1 + \mathrm{A}_1 E_v}. \tag{30}$$

Expressions (16)–(30) fully formulate the STEC model for thermodynamically consistent calculations of the properties of matter over a wide range of changes in internal energy and entropy.

3. Thermodynamic Characteristics of Aluminum in Shock Waves

The results of the calculations of shock compressibility of aluminum using the STEC model with constants that were previously proposed [77,86,87] for the TEC model expressions are presented below. The values of the constants used are as follows: $\rho_0 = 2.71$ g/cm^3, $A = 24.57$ GPa, $n = 3.1$, $C_{V0} = 1$ J/[g K], $\Gamma_0 = 2.13$, $\Gamma_1 = 1.25$, $\Gamma_\infty = 0.3$, $T_0 = 0.3$ kK and $T_1 = 23$ kK. When calculating, it is set that $V_0 = 1/\rho_0$ and $S_0 = 0$.

The shock compressibility of aluminum has been investigated over a wide range of pressures [51,111–134]. In these experiments, various loading means have been used, including traditional planar explosive devices [48,135], layered cumulative systems [124,136] and converging-shock-wave explosive generators [135,137,138], as well as gas guns [121,139,140]. Underground nuclear explosions [49,141–143], laser pulses [16,17,21–24,144] and magnetic fields [10,130,140,145] have also been used to generate shock waves in aluminum samples. Here, the initial porosity of the samples (ρ_0/ρ_{00}, where ρ_{00} is the initial density of the samples) is varied from 1 to 8.

For comparison with these experimental data, the parameters of the shock adiabats were calculated by solving a system of equations, including the equation of state and the expression for the law of conservation of energy of matter through the shock-wave front [1]:

$$E = E_0 + 2^{-1}(P + P_0)(V_{00} - V), \tag{31}$$

where E, P and V are the specific internal energy, pressure and specific volume of the substance behind the front, and E_0, P_0 and V_{00} are the same parameters ahead of the front.

The velocity of the shock-wave front (U_s, the shock velocity) and the velocity of the substance behind the front (U_p, the particle velocity) are determined from the laws of conservation of mass and momentum through the shock-wave front [1] in the following form:

$$U_s = V_{00}\sqrt{\frac{P - P_0}{V_{00} - V}}, \tag{32}$$

$$U_p = \sqrt{(P - P_0)(V_{00} - V)}. \tag{33}$$

In the selected initial state for relations (31)–(33), the pressure is assumed to be $P_0 = 0.1$ MPa and the internal energy is found from the equation of state, $E_0 = E(V_0, S_{\text{in}})$, where the entropy at the initial point S_{in} is given by the condition $P_0 = P(V_0, S_{\text{in}})$ and $V_{00} = 1/\rho_{00}$.

The results of calculations of the parameters of shock compression of aluminum using the STEC model for samples with $\rho_{00} = 2.71$, 2.676, 2.607, 1.92, 1.89, 1.816, 1.585, 1.35, 1.3, 0.909, 0.77 and 0.34 g/cm^3 are presented in Figures 1–3 in comparison with experimental data [51,111–134].

One can see that, in the considered pressure range up to 1 TPa, the shock adiabats calculated using the presented STEC model with constants from [77,86,87] are in good agreement with the data from shock-wave experiments [51,111–134].

In Figures 1–3, shock (Hugoniot) adiabats calculated using the equation of state for aluminum [92] within the framework of the KEOS2M model are also shown. The KEOS2M model [9,25,33,92,99,100] is defined in the form of pressure as a function of volume and internal energy (2). In this case, the parameters of the states on the shock adiabats are found by solving the system of two equations: (31) and (2). In the initial state, the pressure in front of the shock wave is assumed to be $P_0 = 0.1$ MPa, and the internal energy E_0 is found from the condition $P_0 = P(V_0, E_0)$.

Analysis of the calculated curves and experimental points drawn in Figures 1–3 shows that, in the considered pressure range up to 1 TPa, the both STEC and KEOS2M models give results close to each other and to experiments for non-porous samples of aluminum. With increasing porosity of the samples, the difference becomes noticeable already at pressures up to 100 GPa.

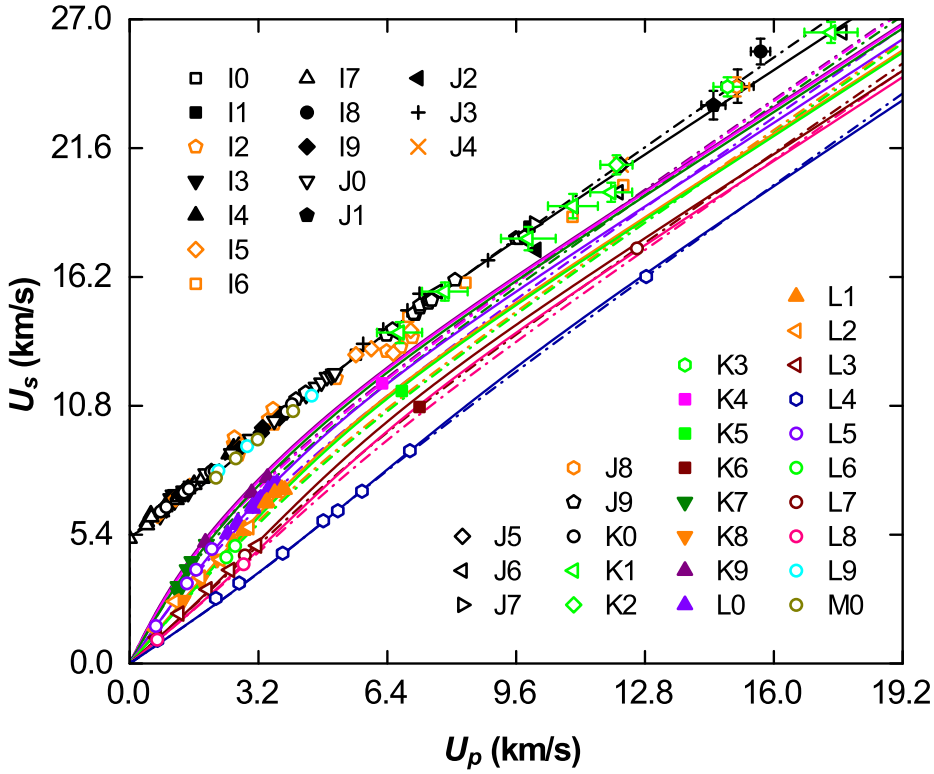

Figure 1. Shock (Hugoniot) adiabats of aluminum samples with different initial densities (ρ_{00}): solid and dash-dot lines—the results of present calculations using the STEC (solid lines) and KEOS2M (Adapted from Ref. [92]) (dash-dot lines) models for ρ_{00} = 2.71, 1.92, 1.89, 1.816, 1.585, 1.35, 1.3, 0.909, 0.77 and 0.34 g/cm^3 (for adiabats from top to bottom); markers—experimental data for solid (I0—Adapted from Ref. [111]; I1—Adapted from Ref. [112]; I2—Adapted from Ref. [113]; I3—Adapted from Ref. [114]; I4—Adapted from Ref. [115]; I5—Adapted from Ref. [116]; I6—Adapted from Ref. [117]; I7—Adapted from Ref. [118]; I8—Adapted from Ref. [119]; I9—Adapted from Ref. [120]; J0—Adapted from Ref. [121]; J1—Adapted from Ref. [122]; J2—Adapted from Ref. [123]; J3—Adapted from Ref. [124]; J4—Adapted from Ref. [125]; J5—Adapted from Ref. [126]; J6—Adapted from Ref. [127], interpretation of data from [128]; J7—Adapted from Ref. [127]; J8—Adapted from Ref. [129]; J9—Adapted from Ref. [130]; K0—Adapted from Ref. [131]; K1—Adapted from Ref. [51], interpretation of data from [128]; K2—Adapted from Ref. [51], interpretation of data from [125,126]; K3—Adapted from Ref. [51], interpretation of data from [129]) and porous samples (K4, K5 and K6—Adapted from Ref. [112]; K7 and K8—Adapted from Ref. [114]; K9, L0 and L1—Adapted from Ref. [115]; L2 and L3—Adapted from Ref. [132]; L4—Adapted from Ref. [133]; L5, L6, L7 and L8—Adapted from Ref. [131]; L9 and M0—Adapted from Ref. [134]; lines and markers of the same color correspond to the same initial density).

In general, the equations of state within the framework of the STEC and KEOS2M models are in good agreement with the set of available shock-wave data for both solid [51,111–131] and porous samples [112,114,115,131–134] of aluminum; differences appear at pressures higher than those achieved experimentally for a fixed initial density, or above 1 TPa. It can be assumed that this is due to the fact that the Grüneisen coefficient $\gamma = V(\partial P/\partial E)_V$ according the STEC model depends only upon the thermal part of the internal energy, whereas this coefficient γ according the KEOS2M model explicitly depends upon both the thermal part of the internal energy and the specific volume.

It should be noted that the proposed STEC equation-of-state model does not take into account possible phase transformations of the metal within the range of thermodynamic parameters under consideration. Examples of equations of state for aluminum that take melting and evaporation into account can be found elsewhere.

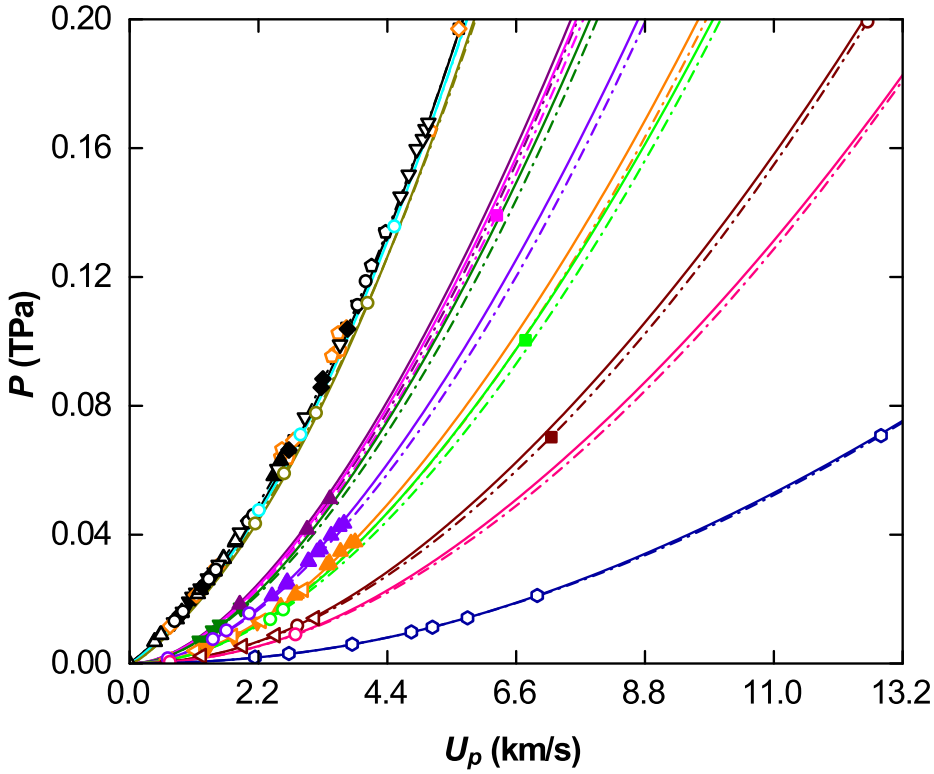

Figure 2. Shock adiabats of aluminum samples with different initial densities: lines—the results of the present calculations for ρ_{00} = 2.71, 2.676, 2.607, 1.92, 1.89, 1.816, 1.585, 1.35, 1.3, 0.909, 0.77 and 0.34 g/cm^3 (for adiabats from top to bottom); the rest of the designations are the same as in Figure 1.

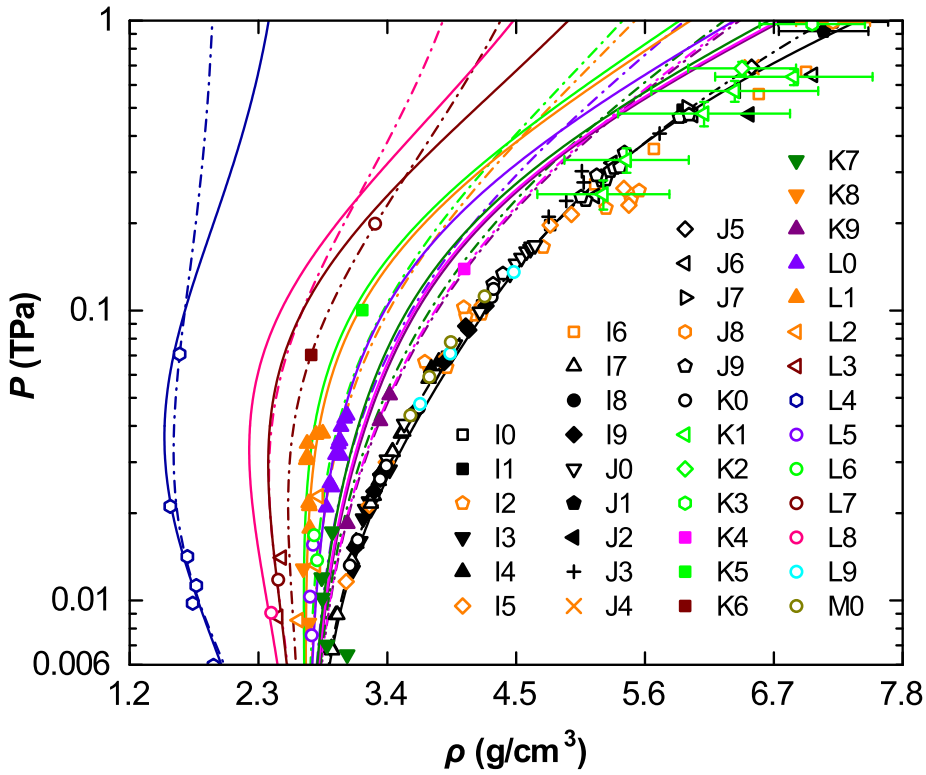

Figure 3. Shock adiabats of aluminum samples with different initial densities: lines—the results of the present calculations for ρ_{00} = 2.71, 1.92, 1.89, 1.816, 1.585, 1.35, 1.3, 0.909, 0.77 and 0.34 g/cm^3 (for adiabats from right to left); the rest of the designations are the same as in Figure 1.

4. Conclusions

Thus, the STEC model proposed in this work makes it possible to describe the properties of matter in a thermodynamically consistent manner within the framework of an unusual thermodynamic potential of specific volume, for which the variables are the entropy and the thermal part of the internal energy. For aluminum, the present equation of state based on fairly simple expressions of the STEC model with constants previously proposed for the TEC model demonstrates good agreement with the data of shock-wave experiments in the pressure range up to 1 TPa. Taking into account possible phase transformations of the metal in this range of achievable parameters remains outside the scope of the STEC model. The developed STEC model can be used in numerical simulations of hydrodynamics of various physical processes at high entropies and energy densities.

Author Contributions: Conceptualization, K.V.K., K.A.B., L.R.O. and N.N.S.; methodology, K.V.K., K.A.B., L.R.O. and N.N.S.; software, K.V.K., K.A.B., L.R.O. and N.N.S.; validation, K.V.K., K.A.B., L.R.O. and N.N.S.; formal analysis, K.V.K., K.A.B., L.R.O. and N.N.S.; investigation, K.V.K., K.A.B., L.R.O. and N.N.S.; resources, K.V.K., K.A.B., L.R.O. and N.N.S.; data curation, K.V.K., K.A.B., L.R.O. and N.N.S.; writing—original draft preparation, K.V.K., K.A.B., L.R.O. and N.N.S.; writing—review and editing, K.V.K., K.A.B., L.R.O. and N.N.S.; visualization, K.V.K., K.A.B., L.R.O. and N.N.S.; supervision, K.V.K.; project administration, K.V.K.; funding acquisition, K.V.K. All authors have read and agreed to the published version of the manuscript.

Funding: The present work is supported by the Ministry of Science and Higher Education of the Russian Federation (state assignment No. 075-00269-25-00 of 26 December 2024).

Data Availability Statement: The original contributions presented in this study are included in the article. Further inquiries can be directed to the corresponding author.

Acknowledgments: The authors are grateful to S. A. Kinelovskii and K. K. Maevskii for constructive discussion of the results of the work.

Conflicts of Interest: The authors declare no conflicts of interest.

Appendix A. Thermodynamic Inconsistency of the TEC Model

The thermodynamic inconsistency of equations of state (3) and (4) can be illustrated by a dimensionless parameter that is obtained by dividing one term on the left-hand side of relation (15) by the sum of the other two or dividing the sum of two such terms by the remaining one, adding the unit and taking the absolute value of the result. This can be performed in six different ways.

Therefore one obtains six different dimensionless parameters, which in the case of the thermodynamic consistency of equations of state (3) and (4) must be equal to zero:

$$\kappa_1 = \left| 1 + \frac{(\partial E/\partial V)_T}{P - T(\partial P/\partial T)_V} \right|, \tag{A1}$$

$$\kappa_2 = \left| 1 + \frac{P - T(\partial P/\partial T)_V}{(\partial E/\partial V)_T} \right|, \tag{A2}$$

$$\kappa_3 = \left| 1 - \frac{T(\partial P/\partial T)_V}{(\partial E/\partial V)_T + P} \right|, \tag{A3}$$

$$\kappa_4 = \left| 1 - \frac{(\partial E/\partial V)_T + P}{T(\partial P/\partial T)_V} \right|, \tag{A4}$$

$$\kappa_5 = \left| 1 + \frac{P}{(\partial E/\partial V)_T - T(\partial P/\partial T)_V} \right|, \tag{A5}$$

$$\kappa_6 = \left| 1 + \frac{(\partial E/\partial V)_T - T(\partial P/\partial T)_V}{P} \right|. \tag{A6}$$

The results of the present calculations of the inconsistency parameters κ_1 (A1) to κ_6 (A6) in states on the shock adiabats of samples with different initial densities for aluminum according to the TEC model [77,86,87] are shown in Figure A1.

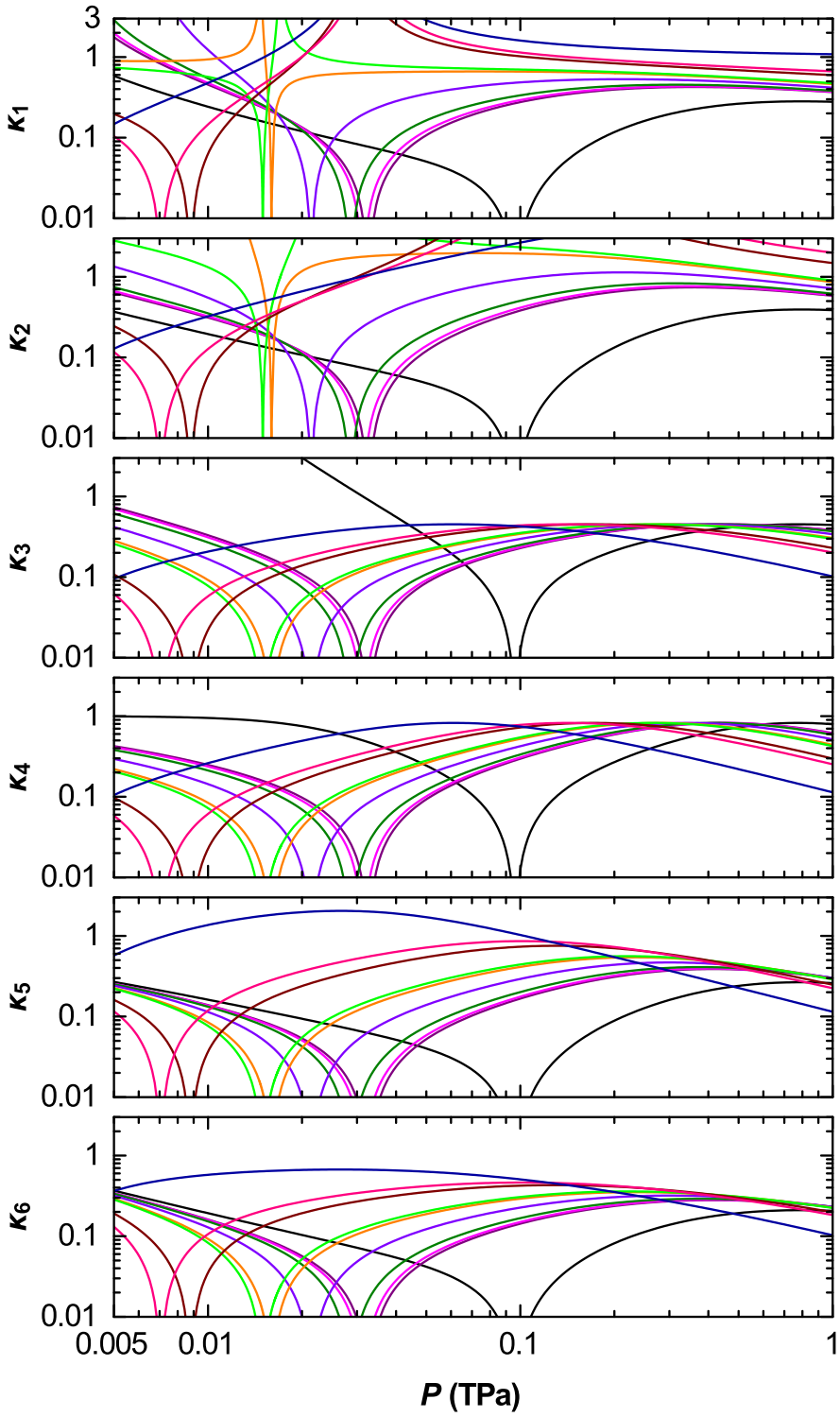

Figure A1. The inconsistency parameters κ_1 to κ_6 (for diagrams from top to bottom) as functions of pressure for shock adiabats of aluminum samples with initial densities ρ_{00} = 2.71, 1.92, 1.89, 1.816, 1.585, 1.35, 1.3, 0.909, 0.77 and 0.34 g/cm^3 calculated using the TEC model (Adapted from Refs. [77,86,87]): the colors of the lines correspond to the curves in Figures 1–3.

In this case, the calculation of the Hugoniot parameters is carried out by solving a system of three equations: (31), (3) and (4), where the last two equations of state are given by the expressions (6)–(13) with constants from [77,86,87]. At the initial point of the calculated shock adiabats (31), the pressure is assumed to be $P_0 = 0.1$ MPa, and the internal energy is found from the equation of state, $E_0 = E(V_0, T_{\text{in}})$, where the temperature at the initial point T_{in} is specified by the condition $P_0 = P(V_0, T_{\text{in}})$.

It should be noted that the parameters of shock-compressed aluminum calculated in this way, included in the expressions (31)–(33), namely, E, P, V, U_s and U_p, according to the TEC model [77,86,87] exactly coincide with the results of calculations according to the STEC model, shown in Figures 1–3.

The results shown in Figure A1 demonstrate a significant thermodynamic inconsistency of the equation of state for aluminum within the TEC model [77,86,87] in the pressure range from 5 GPa to 1 TPa.

References

1. Zel'dovich, Y.B.; Raizer, Y.P. *Physics of Shock Waves and High-Temperature Hydrodynamic Phenomena*; Academic Press: New York, NY, USA, 1967.
2. Bushman, A.V.; Fortov, V.E.; Kanel', G.I.; Ni, A.L. *Intense Dynamic Loading of Condensed Matter*; Taylor & Francis: Washington, DC, USA, 1993.
3. Fortov, V. *Intense Shock Waves on Earth and in Space*; Springer: Cham, Switzerland, 2021. https://doi.org/10.1007/978-3-030-74840-1.
4. Agureikin, V.A.; Anisimov, S.I.; Bushman, A.V.; Kanel', G.I.; Karyagin, V.P.; Konstantinov, A.B.; Kryukov, B.P.; Minin, V.F.; Razorenov, S.V.; Sagdeev, R.Z.; et al. Thermo-physical and gas-dynamic studies of the meteorite shield for the Vega spacecraft. *High Temp.* **1984**, *22*, 761–778.
5. Povarnitsyn, M.E.; Khishchenko, K.V.; Levashov, P.R. Hypervelocity impact modeling with different equations of state. *Int. J. Impact Eng.* **2006**, *33*, 625–633. https://doi.org/10.1016/j.ijimpeng.2006.09.078.
6. Povarnitsyn, M.E.; Khishchenko, K.V.; Levashov, P.R. Simulation of shock-induced fragmentation and vaporization in metals. *Int. J. Impact Eng.* **2008**, *13*, 1723–1727. https://doi.org/10.1016/j.ijimpeng.2008.07.011.
7. Charakhch'yan, A.A.; Khishchenko, K.V.; Fortov, V.E.; Frolova, A.A.; Milyavskiy, V.V.; Shurshalov, L.V. Shock compression of some porous media in conical targets: Numerical study. *Shock Waves* **2011**, *21*, 35–42. https://doi.org/10.1007/s00193-010-0274-y.
8. Khishchenko, K.V.; Charakhch'yan, A.A.; Fortov, V.E.; Frolova, A.A.; Milyavskiy, V.V.; Shurshalov, L.V. Hydrodynamic simulation of converging shock waves in porous conical samples enclosed within solid targets. *J. Appl. Phys.* **2011**, *110*, 053501. https://doi.org/10.1063/1.3605556.
9. Popova, T.V.; Mayer, A.E.; Khishchenko, K.V. Evolution of shock compression pulses in polymethylmethacrylate and aluminum. *J. Appl. Phys.* **2018**, *123*, 235902. https://doi.org/10.1063/1.5029418.
10. Aleksandrov, V.V.; Branitskii, A.V.; Grabovski, E.V.; Laukhin, Y.N.; Oleinik, G.M.; Tkachenko, S.I.; Frolov, I.N.; Khishchenko, K.V. Study of the impact of a duralumin flyer with a tungsten target at the Angara-5-1 facility. *Plasma Phys. Rep.* **2019**, *45*, 421–426. https://doi.org/10.1134/S1063780X19040019.
11. Khishchenko, K.V.; Mayer, A.E. High- and low-entropy layers in solids behind shock and ramp compression waves. *Int. J. Mech. Sci.* **2021**, *189*, 105971. https://doi.org/10.1016/j.ijmecsci.2020.105971.
12. Wen, K.; Chen, X.W.; Lu, Y.G. Research and development on hypervelocity impact protection using Whipple shield: An overview. *Def. Technol.* **2021**, *17*, 1864–1886. https://doi.org/10.1016/j.dt.2020.11.005.
13. Radchenko, P.A.; Radchenko, A.V.; Batuev, S.P.; Kanutkin, A.V. Application of the finite element method to evaluate the effectiveness of spacecraft protective screens. *Acta Astronaut.* **2025**, *229*, 466–470. https://doi.org/10.1016/j.actaastro.2025.01.045.
14. Rodionov, E.S.; Cherepanov, A.Y.; Fazlitdinova, A.G.; Sultanov, T.T.; Lupanov, V.G.; Mayer, P.N.; Mayer, A.E. Dynamic plasticity and fracture of Al 7075 and V95T1 alloys: High-velocity impact experiments. *Dynamics* **2025**, *5*, 6. https://doi.org/10.3390/dynamics5010006.
15. Abdelmaola, M.; Thurston, B.; Panton, B.; Vivek, A.; Daehn, G. Influence of augmentation compositions and confinement layers on flyer velocity in laser impact welding. *Metals* **2025**, *15*, 190. https://doi.org/10.3390/met15020190.
16. Anisimov, S.I.; Prokhorov, A.M.; Fortov, V.E. The use of powerful lasers for the study of matter under superhigh pressures. *Usp. Fiz. Nauk* **1984**, *142*, 395–434.

17. Batani, D.; Koenig, M.; Benuzzi, A.; Krasyuk, I.K.; Pashinin, P.P.; Semenov, A.Yu.; Lomonosov, I.V.; Fortov, V.E. Problems in the optical measurement of dense plasma heating in laser shock wave compression. *Plasma Phys. Control. Fusion* **1999**, *41*, 93–103. https://doi.org/10.1088/0741-3335/41/1/006.
18. Povarnitsyn, M.E.; Itina, T.E.; Khishchenko, K.V.; Levashov, P.R. Multi-material two-temperature model for simulation of ultra-short laser ablation. *Appl. Surf. Sci.* **2007**, *253*, 6343–6346. https://doi.org/10.1016/j.apsusc.2007.01.103.
19. Abrosimov, S.A.; Bazhulin, A.P.; Voronov, V.V.; Krasyuk, I.K.; Pashinin, P.P.; Semenov, A.Y.; Stuchebryukhov, I.A.; Khishchenko, K.V. Study of mechanical properties of aluminum, AMg6M alloy, and polymethyl methacrylate at high strain rates under the action of picosecond laser radiation. *Dokl. Phys.* **2012**, *57*, 64–66. https://doi.org/10.1134/S1028335812020097.
20. Inogamov, N.A.; Zhakhovsky, V.V.; Khokhlov, V.A.; Demaske, B.J.; Khishchenko, K.V.; Oleynik, I.I. Two-temperature hydrodynamic expansion and coupling of strong elastic shock with supersonic melting front produced by ultrashort laser pulse. *J. Phys. Conf. Ser.* **2014**, *500*, 192023. https://doi.org/10.1088/1742-6596/500/19/192023.
21. Shu, H.; Huang, X.; Ye, J.; Jia, G.; Wu, J.; Fu, S. Absolute equation of state measurement of aluminum using laser quasi-isentropic-driven flyer plate. *Laser Part. Beams* **2017**, *35*, 145–153. https://doi.org/10.1017/S0263034616000896.
22. Gus'kov, S.Y.; Krasyuk, I.K.; Semenov, A.Y.; Stuchebryukhov, I.A.; Khishchenko, K.V. Extraction of the shock adiabat of metals from the decay characteristics of a shock wave in a laser experiment. *JETP Lett.* **2019**, *109*, 516–520. https://doi.org/10.1134/S0021364019080071.
23. Semenov, A.Y.; Stuchebryukhov, I.A.; Khishchenko, K.V. Modeling of shock-wave processes in aluminum under the action of a short laser pulse. *Math. Montis.* **2021**, *50*, 108–118. https://doi.org/10.20948/mathmontis-2021-50-10.
24. Belov, I.A.; Bel'kov, S.A.; Bondarenko, S.V.; Vergunova, G.A.; Voronin, A.Y.; Garanin, S.G.; Golovkin, S.Y.; Gus'kov, S.Y.; Demchenko, N.N.; Derkach, V.N.; et al. Shock-wave pressure transfer to a solid target with porous absorber of high-power laser pulse. *J. Exp. Theor. Phys.* **2022**, *134*, 340–349. https://doi.org/10.1134/S106377612203013X.
25. Semenov, A.Y.; Abrosimov, S.A.; Stuchebryukhov, I.A.; Khishchenko, K.V. Studying the dynamics of wave processes of compression and expansion in palladium under picosecond laser action. *High Temp.* **2023**, *61*, 502–507. https://doi.org/10.1134/S0018151X23040132.
26. Shen, Z.; Xu, Q.; Yu, Y.; Liu, D.; Ji, J. Fabrication of papillary composite microstructured aluminum surfaces by laser shock imprinting and ablation. *Metals* **2024**, *14*, 1346. https://doi.org/10.3390/met14121346.
27. Romashevskiy, S.A.; Ashitkov, S.I.; Khokhlov, V.A.; Inogamov, N.A. Study of energy relaxation in a nickel nanofilm after ultrafast heating of the electronic subsystem by a femtosecond laser pulse. *High Temp.* **2024**, *62*, 795–800. https://doi.org/10.1134/S0018151X25700427.
28. Nakanii, N.; Mori, Y.; Inoue, S.; Sano, T. Ultrafast observation of shock wave formation in aluminum under direct femtosecond laser irradiation. *J. Appl. Phys.* **2025**, *137*, 153108. https://doi.org/10.1063/5.0263267.
29. Weber, M.; Raffray, Y.; Loison, D.; Aubert, B.; Benuzzi-Mounaix, A.; Berthe, L.; Harmand, M.; Jodar, B.; Videau, L.; Vinci, T.; et al. Experimental and numerical investigation of laser intensity distribution influence on laser pressure loading. *J. Appl. Phys.* **2025**, *138*, 033104. https://doi.org/10.1063/5.0273654.
30. Khomich, V.Y.; Shakhmatov, E.V.; Sviridov, K.N. Laser-optical technologies for space debris removal. *Acta Astronaut.* **2025**, *226*, 78–85. https://doi.org/10.1016/j.actaastro.2024.10.027.
31. Bushman, A.V.; Romanov, G.S.; Smetannikov, A.S. Theoretical modeling of the initial-stage of a pulsed layer discharge including the real equation of state of the conductor. *High Temp.* **1984**, *22*, 658–664.
32. Korobenko, V.N.; Rakhel, A.D.; Savvatimski, A.I.; Fortov, V.E. Measurement of the electrical resistivity of hot aluminum passing from the liquid to gaseous state at supercritical pressure. *Phys. Rev. B* **2005**, *71*, 014208. https://doi.org/10.1103/PhysRevB.71.014208.
33. Rososhek, A.; Efimov, S.; Nitishinski, M.; Yanuka, D.; Tewari, S.V.; Gurovich, V.T.; Khishchenko, K.; Krasik, Y.E. Spherical wire arrays electrical explosion in water and glycerol. *Phys. Plasmas* **2017**, *24*, 122705. https://doi.org/10.1063/1.5000037.
34. Oreshkin, E.V.; Barengolts, S.A.; Oreshkin, V.I. The specific current action integral for conductors exploded by high-frequency currents. *Phys. Plasmas* **2024**, *31*, 033904. https://doi.org/10.1063/5.0196939.
35. Yang, L.; Rehwald, M.; Kluge, T.; Laso Garcia, A.; Toncian, T.; Zeil, K.; Schramm, U.; Cowan, T.E.; Huang, L. Dynamic convergent shock compression initiated by return current in high-intensity laser–solid interactions. *Matter Radiat. Extrem.* **2024**, *9*, 047204. https://doi.org/10.1063/5.0181321.
36. Li, Y.; Ren, H.; Liu, S. Influence of the glycidyl azide polymer on the energy release of aluminum sub-micron particles under ultrafast heating rates stimulated by electric explosion and solid laser. *Metals* **2024**, *14*, 786. https://doi.org/10.3390/met14070786.
37. Grikshtas, R.; Asmedianov, N.; Belozerov, O.; Efimov, S.; Strucka, J.; Yao, Y.; Lukic, B.; Rack, A.; Bland, S.N.; Krasik, Y.E. Electrothermal instabilities observed by x-ray radiography of underwater sub-microsecond electrical explosions of aluminum, silver, and molybdenum wires. *Phys. Plasmas* **2025**, *32*, 032705. https://doi.org/10.1063/5.0253598.
38. Bushman, A.V.; Fortov, V.E.; Lomonosov, I.V. Investigations of metals in the liquid and plasma states by use of shock waves. *J. Non-Cryst. Solids* **1993**, *156–158*, 631–638. https://doi.org/10.1016/0022-3093(93)90036-W.

39. Lomonosov, I.V.; Fortova, S.V. Wide-range semiempirical equations of state of matter for numerical simulation on high-energy processes. *High Temp.* **2017**, *55*, 585–610. https://doi.org/10.1134/S0018151X17040113.
40. Maler, D.; Liziakin, G.; Belozerov, O.; Efimov, S.; Rakhmilevich, D.; Cohen, K.; Krasik, Y.E. Comparing magnetic pushing to underwater explosions for flyer acceleration. *J. Appl. Phys.* **2023**, *134*, 185902. https://doi.org/10.1063/5.0176294.
41. Tkachenko, S.I.; Levashov, P.R.; Khishchenko, K.V. Analysis of electrical conductivity measurements in strongly coupled tungsten and aluminum plasmas. *Czech. J. Phys.* **2006**, *56*, B419–B424. https://doi.org/10.1007/s10582-006-0232-1.
42. Tkachenko, S.I.; Levashov, P.R.; Khishchenko, K.V. The influence of an equation of state on the interpretation of electrical conductivity measurements in strongly coupled tungsten plasma. *J. Phys. A Math. Gen.* **2006**, *39*, 7597–7603. https://doi.org/10.1088/0305-4470/39/23/028.
43. Hangai, Y.; Kaneko, Y.; Amagai, K. Continuous fabrication process of aluminum foam from foaming to press forming. *Metals* **2025**, *15*, 633. https://doi.org/10.3390/met15060633.
44. Bushman, A.V.; Fortov, V.E. Models of equation of the matter state. *Usp. Fiz. Nauk* **1983**, *140*, 177–232.
45. Khishchenko, K.V. The equation of state for magnesium at high pressures. *Tech. Phys. Lett.* **2004**, *30*, 829–831. https://doi.org/10.1134/1.1813723.
46. Mead, P.T.; Rogers, J.A.; Williams, T.N.; Wilkerson, J.W.; Lacy, T.E., Jr. EPIC simulations of hypervelocity impacts of aluminum spheres into high-density polyethylene plates. *J. Dynamic Behavior Mater.* **2025**. https://doi.org/10.1007/s40870-025-00484-8.
47. Kolgatin, S.N.; Khachatur'yants, A.V. Interpolation equations of state of metals. *High Temp.* **1982**, *20*, 380–384.
48. Al'tshuler, L.V. Use of shock waves in high-pressure physics. *Usp. Fiz. Nauk* **1965**, *85*, 197–258.
49. Trunin, R.F. Shock compression of condensed matters in strong shock-waves caused by underground nuclear-explosions. *Usp. Fiz. Nauk* **1994**, *164*, 1215–1237.
50. Kadatskiy, M.A.; Khishchenko, K.V. Comparison of Hugoniots calculated for aluminum in the framework of three quantum-statistical models. *J. Phys. Conf. Ser.* **2015**, *653*, 012079. https://doi.org/10.1088/1742-6596/653/1/012079.
51. Orlov, N.Y.; Kadatskiy, M.A.; Denisov, O.B.; Khishchenko, K.V. Application of quantum-statistical methods to studies of thermodynamic and radiative processes in hot dense plasmas. *Matter Radiat. Extrem.* **2019**, *4*, 054403. https://doi.org/10.1063/1.5096439.
52. Karakulov, V.V.; Skripnyak, V.A. About mechanical behavior and effective properties of metal matrix composites under shock wave loading. In *Behavior of Materials Under Impact, Explosion, High Pressures and Dynamic Strain Rates*; Orlov, M.Y., Visakh, P.M., Eds.; Advanced Structured Materials; Springer: Cham, Switzerland, 2023; Volume 176, pp. 53–68. https://doi.org/10.1007/978-3-031-17073-7_4.
53. Cao, R.; Chen, J.; Song, X.; Feng, D.; Peng, C.; Li, Z. Numerical simulation of the damage characteristics of carbon fiber-reinforced aluminum laminates under hypervelocity impact based on the FE-SPH adaptive method. *Appl. Compos. Mater.* **2025**, *32*, 817–847. https://doi.org/10.1007/s10443-024-10303-3.
54. Zou, G.; Yang, Y.; Chang, Z.; Wu, S.; Wang, X. Analytical and numerical investigation on the penetration resistance of PUE/honeycomb aluminum composite structures. *Acta Mech. Solida Sin.* **2024**, *37*, 771–785. https://doi.org/10.1007/s10338-024-00477-5.
55. Dadoura, M.H.; Farahat, A.I.Z.; Taha, M.R.; Elshaer, R.N. Enhancement of quasi-static compression strength for aluminum closed cell foam blocks shielded by aluminum tubes. *Sci. Rep.* **2023**, *13*, 6929. https://doi.org/10.1038/s41598-023-33750-7.
56. Wu, F.; Miao, B.; Tian, Y.; Zhang, F.; Zhang, C. Aluminum foam as buffer layer used in soft rock tunnel with large deformation. *J. Mt. Sci.* **2025**, *22*, 324–336. https://doi.org/10.1007/s11629-024-9072-3.
57. Hao, T.; Yang, X.; Xie, A.; Deng, S.; Yu, B.; Sun, Q. A novel aluminum foam structure for combined excellent wave attenuation and ventilation performance. *Sci. Rep.* **2025**, *15*, 7346. https://doi.org/10.1038/s41598-025-91556-1.
58. Thorat, M.; Kumar, G.; Sahu, S.N.; Menezes, V.; Gokhale, A.A. Cell wall fracture in shock-loaded aluminum foams. *J. Mater. Eng. Perform.* **2025**, *34*, 10810–10818. https://doi.org/10.1007/s11665-024-09878-6.
59. Shepelev, V.V. Hydrodynamic modeling of laser-induced shock waves in aluminum in a cylindrically symmetric statement. *J. Appl. Ind. Math.* **2023**, *17*, 385–395. https://doi.org/10.1134/S1990478923020163.
60. Sharma, A.; Song, J.; Furfari, D.; Mannava, S.R.; Vasudevan, V.K. Influence of laser shock peening and ultrasonic nanocrystal surface modification on residual stress, microstructure, and corrosion–fatigue behavior of aluminum 7075-T6. *Metall. Mater. Trans. A* **2023**, *54*, 4233–4252. https://doi.org/10.1007/s11661-023-07159-w.
61. Bakulin, I.A.; Kuznetsov, S.I.; Panin, A.S.; Tarasova, E.Y.; Yaresko, S.I.; Novikov, V.A. Effect of preliminary heat treatment on the formation of structure and residual stresses in the AMg6 alloy at laser shock peening without coating. *J. Russ. Laser Res.* **2024**, *45*, 237–248. https://doi.org/10.1007/s10946-024-10207-4.
62. Meng, X.; Cheng, Z.; Zhou, J.; Song, F.; Zhao, X.; Wu, W.; Gao, F.; Cai, J.; Xue, W.; Liu, Y. Study on the wear resistance of 2024-T351 aluminum alloy strengthened by ultrasonic-assisted laser shock peening. *J. Mater. Sci.* **2025**, *60*, 5954–5976. https://doi.org/10.1007/s10853-025-10786-w.

63. Song, P.F.; Cao, M.Y.; Fu, M.; Li, B.; Wu, L.J.; Li, Y.F.; Liu, Z. Effect of ultrasonic vibration modes on the residual stress relaxation and mechanical properties of aluminum alloy. *J. Cent. South Univ.* **2025**, *32*, 1008–1023. https://doi.org/10.1007/s11771-025-5913-7.
64. Pikuz, S.A.; Tilikin, I.N.; Romanova, V.M.; Mingaleev, A.R.; Shelkovenko, T.A. Development of instabilities in thin aluminum foils exploded using generator with current of up to 10 kA. *Plasma Phys. Rep.* **2024**, *50*, 792–799. https://doi.org/10.1134/S1063780X24600889.
65. Walsh, J.M.; Rice, M.H.; McQueen, R.G.; Yarger, F.L. Shock-wave compressions of twenty-seven metals. Equations of state of metals. *Phys. Rev.* **1957**, *108*, 196–216. https://doi.org/10.1103/PhysRev.108.196.
66. Kormer, S.B.; Urlin, V.D. Interpolation equations for the condition of metals at super high pressures. *Dokl. Akad. Nauk SSSR* **1960**, *131*, 542–545.
67. Leont'ev, A.A.; Fortov, V.E. Melting and evaporation of metals in an unloading wave. *J. Appl. Mech. Tech. Phys.* **1974**, *15*, 417–420. https://doi.org/10.1007/BF00852235.
68. Godwal, B.K.; Sikka, S.K.; Chidambaram, R. Equation of state theories of condensed matter up to about 10 TPa. *Phys. Rep.* **1983**, *102*, 121–197. https://doi.org/10.1016/0370-1573(83)90014-5.
69. Young, D.A.; Wolford, J.K.; Rogers, F.J.; Holian, K.S. Theory of the aluminum shock equation of state to 10^4 Mbar. *Phys. Lett. A* **1985**, *108*, 157–160. https://doi.org/10.1016/0375-9601(85)90849-7.
70. Holian, K.S. A new equation of state for aluminum. *J. Appl. Phys.* **1986**, *59*, 149–157. https://doi.org/10.1063/1.336853.
71. Kerley, G.I. Theoretical equation of state for aluminum. *Int. J. Impact Eng.* **1987**, *5*, 441–449. https://doi.org/10.1016/0734-743X(87)90059-5.
72. Wu, Q.; Jing, F.Q. Thermodynamic equation of state and application to Hugoniot predictions for porous materials. *J. Appl. Phys.* **1996**, *80*, 4343–4349. https://doi.org/10.1063/1.363391.
73. Geng, H.Y.; Wu, Q.; Tan, H.; Cai, L.C.; Jing, F.Q. Extension of the Wu–Jing equation of state for highly porous materials: Calculations to validate and compare the thermoelectron model. *J. Appl. Phys.* **2002**, *92*, 5917–5923. https://doi.org/10.1063/1.1516618.
74. Chisolm, E.D.; Crockett, S.D.; Wallace, D.C. Test of a theoretical equation of state for elemental solids and liquids. *Phys. Rev. B* **2003**, *68*, 104103. https://doi.org/10.1103/PhysRevB.68.104103.
75. Lomonosov, I.V. Multi-phase equation of state for aluminum. *Laser Part. Beams* **2007**, *25*, 567–584. https://doi.org/10.1017/S0263034607000687.
76. Gordeev, D.G.; Gudarenko, L.F.; Zhernokletov, M.V.; Kudel'kin, V.G.; Mochalov, M.A. Semi-empirical equation of state of metals. Equation of state of aluminum. *Combust. Explos. Shock Waves* **2008**, *44*, 177–189. https://doi.org/10.1007/s10573-008-0024-y.
77. Kinelovskii, S.A.; Maevskii, K.K. Simple model for calculating shock adiabats of powder mixtures. *Combust. Explos. Shock Waves* **2011**, *47*, 706–714. https://doi.org/10.1134/S001050821106013X.
78. Medvedev, A.B.; Trunin, R.F. Shock compression of porous metals and silicates. *Phys. Usp.* **2012**, *55*, 773–789. https://doi.org/10.3367/UFNe.0182.201208b.0829.
79. Liu, H.; Song, H.; Zhang, G. The single phase and two-phase equations of state for aluminum. *AIP Conf. Proc.* **2012**, *1426*, 832–835. https://doi.org/10.1063/1.3686407.
80. Minakov, D.V.; Levashov, P.R.; Khishchenko, K.V. First-principle simulation of shock-wave experiments for aluminum. *AIP Conf. Proc.* **2012**, *1426*, 836–839. https://doi.org/10.1063/1.3686408.
81. Shemyakin, O.P.; Levashov, P.R.; Khishchenko, K.V. Equation of state of Al based on the Thomas–Fermi model. *Contrib. Plasma Phys.* **2012**, *52*, 37–40. https://doi.org/10.1002/ctpp.201100090.
82. Mishra, V.; Chaturvedi, S. Equation of state of Al for compressed and expanded states from first-principles calculations. *Phys. B* **2012**, *407*, 2533–2537. https://doi.org/10.1016/j.physb.2012.03.062.
83. Li, Y.H.; Chang, J.Z.; Li, X.M.; Zhang, L. Multiphase equation of states of the solid and liquid phases of Al and Ta. *Chin. Phys. Lett.* **2012**, *29*, 046201. https://doi.org/10.1088/0256-307X/29/4/046201.
84. Gordeev, D.G.; Gudarenko, L.F.; Kayakin, A.A.; Kudel'kin, V.G. Equation of state model for metals with ionization effectively taken into account. Equation of state of tantalum, tungsten, aluminum and beryllium. *Combust. Explos. Shock Waves* **2013**, *49*, 92–104. https://doi.org/10.1134/S0010508213010103.
85. Minakov, D.V.; Levashov, P.R.; Khishchenko, K.V.; Fortov, V.E. Quantum molecular dynamics simulation of shock-wave experiments in aluminum. *J. Appl. Phys.* **2014**, *115*, 223512. https://doi.org/10.1063/1.4882299.
86. Kinelovskii, S.A.; Maevskii, K.K. Model of the behavior of aluminum and aluminum-based mixtures under shock-wave loading. *High Temp.* **2014**, *52*, 821–829. https://doi.org/10.1134/S0018151X14050083.
87. Kinelovskii, S.A.; Maevskii, K.K. Estimation of the thermodynamic parameters of a shock-wave action on high-porosity heterogeneous materials. *Tech. Phys.* **2016**, *61*, 1244–1249. https://doi.org/10.1134/S1063784216080144.
88. Wang, K.; Zhang, D.; Shi, Z.Q.; Shi, Y.J.; Wang, T.H.; Zhang, Y. Equation of state for aluminum in warm dense matter regime. *Chin. Phys. B* **2019**, *28*, 016401. https://doi.org/10.1088/1674-1056/28/1/016401.

89. Gilev, S.D. Low-parametric equation of state of aluminum. *High Temp.* **2020**, *58*, 166–172. https://doi.org/10.1134/S0018151X20020078.
90. Bogdanova, Y.A.; Gubin, S.A.; Maklashova, I.V. Calculation of thermodynamic properties of metals and their binary alloys by the perturbation theory. *Metals* **2021**, *11*, 1548. https://doi.org/10.3390/met11101548.
91. Kozyrev, N.V.; Gordeev, V.V. Thermodynamic properties and equation of state for solid and liquid aluminum. *Metals* **2022**, *12*, 1346. https://doi.org/10.3390/met12081346.
92. Khishchenko, K.V. Equation of state for aluminum at high pressures. *High Temp.* **2023**, *61*, 440–443. https://doi.org/10.1134/S0018151X23030227.
93. Wu, M.Z.; Zhang, Q.M.; Zhong, X.Z.; Ren, S.Y. An improved multiphase equation of state for aluminum in hypervelocity impact. *Int. J. Impact Eng.* **2024**, *192*, 105031. https://doi.org/10.1016/j.ijimpeng.2024.105031.
94. Belkheeva, R.K. A simple equation of state for describing the behavior of solid and porous aluminum samples under shock compression and isentropic unloading. *Zh. Tekh. Fiz.* **2025**, *95*, 1303–1312.
95. Zhao, Y.; Wang, L.F.; Zhang, Q.; Zhang, L.; Song, H.; Gao, X.; Sun, B.; Liu, H.; Song, H. A thermodynamically complete multi-phase equation of state for dense and porous metals at wide ranges of temperature and pressure. *Chin. Phys. B* **2025**, *34*, 036401. https://doi.org/10.1088/1674-1056/ada54b.
96. Anand, R.K. On the convergence of strong cylindrical and spherical shock waves in solid materials. *Proc. Natl. Acad. Sci. India Sect. A* **2025**, *95*, 103–112. https://doi.org/10.1007/s40010-025-00909-y.
97. Fortov, V.E. Equations of state of condensed media. *J. Appl. Mech. Tech. Phys.* **1972**, *13*, 894–902. https://doi.org/10.1007/BF01200549.
98. Bushman, A.V.; Lomakin, B.N.; Sechenov, V.A.; Fortov, V.E.; Shchekotov, O.E.; Sharipdzhanov, I.I. Thermodynamics of nonideal cesium plasma. *Zh. Eksp. Teor. Fiz.* **1975**, *69*, 1624–1632.
99. Lomonosov, I.V.; Fortov, V.E.; Khishchenko, K.V. Model of wide-range equations of polymer materials state under high-energy densities. *Khim. Fiz.* **1995**, *14 (1)*, 47–52.
100. Khishchenko, K.V. Equation of state for titanium at high pressures. *High Temp.* **2024**, *62*, 150–153. https://doi.org/10.1134/S0018151X24700196.
101. Seredkin, N.N.; Khishchenko, K.V. Equation of state for the hafnium–zirconium alloy at high pressures and temperatures in shock waves. *High Temp.* **2024**, *62*, 450–453. https://doi.org/10.1134/S0018151X25700038.
102. Boyarskikh, K.A.; Khishchenko, K.V. Algorithm for finding parameters of equations of state by particle swarm optimization. *Bull. Russ. Acad. Sci. Phys.* **2024**, *88*, 1446–1451. https://doi.org/10.1134/S1062873824707670.
103. Bazarov, I.P. *Thermodynamics*; MacMillan: New York, NY, USA, 1964.
104. Charakhch'yan, A.A.; Gryn', V.I.; Khishchenko, K.V. On the role of heat conduction in the formation of a high-temperature plasma during counter collision of rarefaction waves of solid deuterium. *J. Appl. Mech. Tech. Phys.* **2011**, *52*, 501–516. https://doi.org/10.1134/S0021894411040018.
105. Bushman, A.V.; Fortov, V.E.; Sharipdzhanov, I.I. Equation of state for metals in a wide range of parameters. *Teplofiz. Vys. Temp.* **1977**, *15*, 1095–1097.
106. Kinelovskii, S.A.; Maevskii, K.K. Modeling shock loading of multicomponent materials including bismuth. *High Temp.* **2016**, *54*, 675–681. https://doi.org/10.1134/S0018151X16050163.
107. Maevskii, K.K.; Kinelovskii, S.A. Thermodynamic parameters of mixtures with silicon nitride under shock-wave impact in terms of equilibrium model. *High Temp.* **2018**, *56*, 853–858. https://doi.org/10.1134/S0018151X18060172.
108. Maevskii, K.K. Numerical study of shock-wave loading of the W- and WC-based metal composites. *Tech. Phys.* **2021**, *66*, 749–754. https://doi.org/10.1134/S1063784221050145.
109. Maevskii, K.K. Modeling of shock wave loading FeO to 1000 GPa. *J. Appl. Phys.* **2025**, *137*, 055901. https://doi.org/10.1063/5.0233540.
110. Murnaghan, F.D. The compressibility of media under extreme pressures. *Proc. Natl. Acad. Sci. USA* **1944**, *30*, 244–247. https://doi.org/10.1073/pnas.30.9.244.
111. Al'tshuler, L.V.; Kormer, S.B.; Bakanova, A.A.; Trunin, R.F. Equation of state for aluminum, copper, and lead in the high-pressure region. *Zh. Eksp. Teor. Fiz.* **1960**, *38*, 790–798.
112. Kormer, S.B.; Funtikov, A.I.; Ulrin, V.D.; Kolesnikova, A.N. Dynamic compression of porous metals and the equation of state with variable specific heat at high temperatures. *Zh. Eksp. Teor. Fiz.* **1962**, *42*, 686–702.
113. Skidmore, I.C.; Morris, E. Experimental equation-of-state data for uranium and its interpretation in the critical region. In *Thermodynamics of Nuclear Materials*; IAEA: Vienna, Austria, 1962; pp. 173–216.
114. Morgan, D.T.; Rockowitz, M.; Atkinson, A.L. *Measurement of the Grueneisen Parameter and the Internal Energy Dependence of the Solid Equation of State for Aluminum and Teflon*; Tech. Rep. AFWL-TR-65-117; Air Force Weapons Laboratory, Kirtland Air Force Base: Albuquerque, NM, USA, 1965.

115. Anderson, G.D.; Doran, D.G.; Fahrenbruch, A.L. *Equation of State of Solids: Aluminum and Teflon*; Tech. Rep. AFWL-TR-65-147; Air Force Weapons Laboratory, Kirtland Air Force Base: Albuquerque, NM, USA, 1965.
116. Al'tshuler, L.V.; Chekin, B.S. Metrology of high impulse pressure. In *Reports of the 1st All-Union Symposium on Pulse Pressures*; VNIIFTRI: Moscow, USSR, 1974; Volume 1, pp. 5–22.
117. Al'tshuler, L.V.; Kalitkin, N.N.; Kuz'mina, L.V.; Chekin, B.S. Shock adiabats for ultrahigh pressures. *Zh. Eksp. Teor. Fiz.* **1977**, *72*, 317–325.
118. Marsh, S.P. (Ed.) *LASL Shock Hugoniot Data*; University of California Press: Berkeley, CA, USA, 1980.
119. Volkov, L.P.; Voloshin, N.P.; Vladimirov, A.S.; Nogin, V.N.; Simonenko, V.A. Shock compressibility of aluminum at a pressure of 10 Mbar. *JETP Lett.* **1980**, *31*, 588–592.
120. Al'tshuler, L.V.; Bakanova, A.A.; Dudoladov, I.P.; Dynin, E.A.; Trunin, R.F.; Chekin, B.S. Shock adiabatic curves of metals. New data, statistical analysis, and general laws. *J. Appl. Mech. Tech. Phys.* **1981**, *22*, 145–169. https://doi.org/10.1007/BF00907938.
121. Mitchell, A.C.; Nellis, W.J. Shock compression of aluminum, copper, and tantalum. *J. Appl. Phys.* **1981**, *52*, 3363–3374. https://doi.org/10.1063/1.329160.
122. Simonenko, V.A.; Voloshin, N.P.; Vladimirov, A.S.; Nagibin, A.P.; Nogin, V.N.; Popov, V.A.; Salnikov, V.A.; Shoidin, Y.A. Absolute measurements of shock compressibility of aluminum at pressures $P \gtrsim 1$ TPa. *Zh. Eksp. Teor. Fiz.* **1985**, *88*, 1452–1459.
123. Trunin, R.F. Compressibility of various substances at high shock pressures: An overview. *Izv. Acad. Sci. USSR. Phys. Solid Earth* **1986**, *22*, 103–114.
124. Glushak, B.L.; Zharkov, A.P.; Zhernokletov, M.V.; Ternovoi, V.Y.; Filimonov, A.S.; Fortov, V.E. Experimental investigation of the thermodynamics of dense plasmas formed from metals at high energy concentrations. *Zh. Eksp. Teor. Fiz.* **1989**, *96*, 1301–1318.
125. Trunin, R.F.; Panov, N.V.; Medvedev, A.B. Shock compressibilities of iron, aluminum and tantalum at terapascal pressures. *Khim. Fiz.* **1995**, *14 (2–3)*, 97–99.
126. Trunin, R.F.; Panov, N.V.; Medvedev, A.B. Shock compressibility of iron, aluminum, and tantalum under terapascal pressures in laboratory conditions. *High Temp.* **1995**, *33*, 328–329.
127. Trunin, R.F.; Podurets, M.A.; Simakov, G.V.; Popov, L.V.; Sevast'yanov, A.G. New data, obtained under strong shock wave conditions from an underground nuclear explosion, on the compressibility of aluminum, plexiglass, and quartz. *Zh. Eksp. Teor. Fiz.* **1995**, *108*, 851–861.
128. Avrorin, E.N.; Vodolaga, B.K.; Voloshin, N.P.; Kovalenko, G.V.; Kuropatenko, V.F.; Simonenko, V.A.; Chernovolyuk, B.T. Experimental study of the influence of electron shell structure on shock adiabats of condensed materials. *Zh. Eksp. Teor. Fiz.* **1987**, *93*, 613–626.
129. Trunin, R.F.; Panov, N.V.; Medvedev, A.B. Compressibility of iron, aluminum, molybdenum, titanium, and tantalum at shock-wave pressures of 1–2.5 TPa. *JETP Lett.* **1995**, *62*, 591–594.
130. Knudson, M.D.; Lemke, R.W.; Hayes, D.B.; Hall, C.A.; Deeney, C.; Asay, J.R. Near-absolute Hugoniot measurements in aluminum to 500 GPa using a magnetically accelerated flyer plate technique. *J. Appl. Phys.* **2003**, *94*, 4420–4431. https://doi.org/10.1063/1.1604967.
131. Trunin, R.F.; Gudarenko, L.F.; Zhernokletov, M.V.; Simakov, G.V. *Experimental Data on Shock Compression and Adiabatic Expansion of Condensed Matter*; RFNC-VNIIEF: Sarov, Russia, 2006.
132. Bakanova, A.A.; Dudoladov, I.P.; Sutulov, Y.N. Shock compressibility of porous tungsten, molybdenum, copper, and aluminum in the low pressure domain. *J. Appl. Mech. Tech. Phys.* **1974**, *15*, 241–245. https://doi.org/10.1007/BF00850666.
133. Trunin, R.F.; Simakov, G.V.; Panov, N.V. Shock compression of porous aluminum and nickel at megabar pressures. *High Temp.* **2001**, *39*, 401–406. https://doi.org/10.1023/A:1017558609033.
134. Song, P.; Cai, L.; Wang, Q.; Zhou, X.; Li, X.; Zhang, Y.; Yuan, S.; Weng, J.; Li, J. Sound velocity, temperature, melting along the Hugoniot and equation of state for two porosity aluminums. *J. Appl. Phys.* **2011**, *110*, 103522. https://doi.org/10.1063/1.3662193.
135. Al'tshuler, L.V.; Trunin, R.F.; Urlin, V.D.; Fortov, V.E.; Funtikov, A.I. Development of high-pressure dynamical measurement techniques in Russia. *Usp. Fiz. Nauk* **1999**, *169*, 323–344.
136. Bushman, A.V.; Krasyuk, I.K.; Pashinin, P.P.; Prokhorov, A.M.; Ternovoi, V.Y.; Fortov, V.E. Dynamic compressibility and thermodynamics of a dense aluminum plasma at megabar pressures. *JETP Lett.* **1984**, *39*, 411–413.
137. Al'tshuler, L.V.; Trunin, R.F.; Krupnikov, K.K.; Panov, N.V. Explosive laboratory devices for shock wave compression studies. *Usp. Fiz. Nauk* **1996**, *166*, 575–581.
138. Funtikov, A.I. Explosive laboratory measurement of the dynamical compressibility of porous substances in the pressure range from 0.1 to 1 TPa. *Usp. Fiz. Nauk* **1997**, *167*, 1119–1120.
139. Zhang, J.; Zhao, L.; Zhang, R.; Yang, G.; Luo, G.; Shen, Q. Equation of state remeasurements for aluminum and copper under low-impact loading. *AIP Adv.* **2023**, *13*, 045202. https://doi.org/10.1063/5.0142851.
140. Gan, Y.; Nan, X.; Wu, D.; Yang, S.; Li, X.; Geng, H.; Shen, Y.; Yu, Y.; Hu, J. Dynamic yield behaviors of aluminum under shock and ramp compression: Experiments and models. *J. Appl. Phys.* **2025**, *137*, 215902. https://doi.org/10.1063/5.0270423.

141. Ragan, C.E., III. Shock compression measurements at 1 to 7 TPa. *Phys. Rev. A* **1982**, *25*, 3360–3375. https://doi.org/10.1103/PhysRevA.25.3360.
142. Ragan, C.E., III. Shock-wave experiments at threefold compression. *Phys. Rev. A* **1984**, *29*, 1391–1402. https://doi.org/10.1103/PhysRevA.29.1391.
143. Avrorin, E.N.; Vodolaga, B.K.; Simonenko, V.A.; Fortov, V.E. High-intensity shock-waves and the extreme states of matter. *Usp. Fiz. Nauk* **1993**, *163*, 1–34.
144. He, Z.; Fang, Z.; Huang, X.; Xie, Z.; Ye, J.; Dong, J.; Shu, H.; Wang, P.; Jia, G.; Zhang, F.; et al. Sound velocity measurement based on laser-induced microflyers. *AIP Adv.* **2024**, *14*, 105315. https://doi.org/10.1063/5.0221689.
145. Al'tshuler, L.V.; Il'kaev, R.I.; Fortov, V.E. Use of powerful shock and detonation waves to study extreme states of matter. *Phys. Usp.* **2021**, *64*, 1167–1179. https://doi.org/10.3367/UFNe.2021.09.039092.

Disclaimer/Publisher's Note: The statements, opinions and data contained in all publications are solely those of the individual author(s) and contributor(s) and not of MDPI and/or the editor(s). MDPI and/or the editor(s) disclaim responsibility for any injury to people or property resulting from any ideas, methods, instructions or products referred to in the content.